

Regulating *PCCA* gene expression by modulation of pseudoexon splicing patterns to rescue enzyme activity in propionic acidemia

Ulrika Simone Spangsberg Petersen,^{1,5} Maja Dembic,^{1,2,3,5} Ainhoa Martínez-Pizarro,⁴ Eva Richard,⁴ Lise Lolle Holm,¹ Jesper Foged Havelund,¹ Thomas Koed Doktor,¹ Martin Røssel Larsen,¹ Nils J. Færgeman,¹ Lourdes Ruiz Desviat,⁴ and Brage Storstein Andresen¹

¹Department of Biochemistry and Molecular Biology and the Villum Center for Bioanalytical Sciences, University of Southern Denmark, 5230 Odense M, Denmark;

²Department of Clinical Genetics, Odense University Hospital, 5000 Odense C, Denmark; ³Department of Mathematics and Computer Science, University of Southern Denmark, 5230 Odense M, Denmark; ⁴Centro de Biología Molecular Severo Ochoa, UAM-CSIC, CEDEM, CIBERER, IdiPaz, Universidad Autónoma de Madrid, 28049 Madrid, Spain

Pseudoexons are nonfunctional intronic sequences that can be activated by deep-intronic sequence variation. Activation increases pseudoexon inclusion in mRNA and interferes with normal gene expression. The *PCCA* c.1285-1416A>G variation activates a pseudoexon and causes the severe metabolic disorder propionic acidemia by deficiency of the propionyl-CoA carboxylase enzyme encoded by *PCCA* and *PCCB*. We characterized this pathogenic pseudoexon activation event in detail and identified hnRNP A1 to be important for normal repression. The *PCCA* c.1285-1416A>G variation disrupts an hnRNP A1-binding splicing silencer and simultaneously creates a splicing enhancer. We demonstrate that blocking this region of regulation with splice-switching antisense oligonucleotides restores normal splicing and rescues enzyme activity in patient fibroblasts and in a cellular model created by CRISPR gene editing. Interestingly, the *PCCA* pseudoexon offers an unexploited potential to upregulate gene expression because healthy tissues show relatively high inclusion levels. By blocking inclusion of the nonactivated wild-type pseudoexon, we can increase both *PCCA* and *PCCB* protein levels, which increases the activity of the heterododecameric enzyme. Surprisingly, we can increase enzyme activity from residual levels in not only patient fibroblasts harboring *PCCA* missense variants but also those harboring *PCCB* missense variants. This is a potential treatment strategy for propionic acidemia.

INTRODUCTION

Pre-mRNA splicing is the process of joining exons through the excision of intervening introns. This process is catalyzed by the spliceosome and controlled by the “splicing code,” which is a network of features that constitutes a complex regulatory environment.^{1,2} The spliceosome recognizes exons from introns through core splicing signals: the 3' and 5' splice sites (3'/ss/5'/ss) and auxiliary splicing regulatory elements (SREs) that can bind splicing regulatory proteins to enhance or silence splicing in the local pre-mRNA region.^{3–5}

Sequence variation that affects the splicing code will affect the outcome of the pre-mRNA splicing process and can cause disease.⁶ Deep-intronic sequence variation can activate pseudoexons, which are nonfunctional intronic sequences delimited by pairs of cryptic splice sites.^{7–9} Pseudoexon activation increases the pseudoexon inclusion level in mRNA and commonly causes loss of function from frameshift and/or formation of premature termination codons (PTCs), which can target the mRNA transcript for degradation by nonsense-mediated mRNA decay (NMD).^{7,8,10}

Propionic acidemia (MIM: 606054) is an autosomal recessive metabolic disorder characterized by the accumulation of toxic metabolites. Patients present with metabolic decompensation and risk developing severe long-term complications affecting different organ systems. Treatment depends on metabolic control through dietary restrictions, but prevention or treatment of the complications is limited.^{11,12} Propionic acidemia occurs by deficiency of propionyl-coenzyme A (CoA) carboxylase (PCC), which is a heterododecamer enzyme composed of six alpha and six beta subunits encoded by *PCCA* and *PCCB*. The PCC enzyme catalyzes the carboxylation of propionyl-CoA to methylmalonyl-CoA in the catabolism of valine, isoleucine, threonine, methionine, odd-chain fatty acids, and cholesterol in mitochondria.¹³ Propionic acidemia is genetically heterogeneous, and PCC deficiency can occur by deleterious sequence variation in *PCCA* or *PCCB*, with missense variants being predominant in both genes.^{14–19}

Activation of an 84-nt pseudoexon (13:100305751-100305834; GRCh38) from intron 14 of the *PCCA* gene (NM_000282) has been

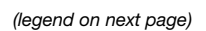
Received 10 July 2023; accepted 8 December 2023;
<https://doi.org/10.1016/j.omtn.2023.102101>.

⁵These authors contributed equally

Correspondence: Professor Brage Storstein Andresen, Department of Biochemistry and Molecular Biology, University of Southern Denmark, Campusvej 55, 5230 Odense M, Denmark.

E-mail: bragea@bmb.sdu.dk





described in a patient with a deep-intronic sequence variation, c.1285-1416A>G (13:100305776; GRCh38).²⁰ Inclusion of the pseudoexon introduces an in-frame PTC, triggering NMD or leading to the translation of a truncated protein. Basal inclusion levels of the *PCCA* pseudoexon have previously been observed in wild-type (WT) cell lines and may represent low-level aberrant splicing that is tolerated by the cell.²¹

In this study, we investigated the mechanism of the pathogenic *PCCA* pseudoexon-activation event in detail to identify efficient splice-switching antisense oligonucleotides (SSOs) that can block the SREs, which are responsible for the inclusion of the pseudoexon in mRNA. Normal inclusion of the nonactivated WT pseudoexon reduces functional gene expression relative to full capability, and we demonstrate that the *PCCA* pseudoexon offers an unexploited potential to upregulate gene expression by the SSO-mediated modulation of pseudoexon splicing patterns. We demonstrate how modulating the levels of the *PCCA* subunit can also be exploited to increase PCC enzyme activity above normal levels by rescue of the unstable excess production of PCCB.^{22,23} Using our most efficient SSO, we can block inclusion of the pseudoexon to increase *PCCA* gene expression, to increase both *PCCA* and PCCB protein levels, resulting in an increase in activity of the multimeric PCC enzyme. This is a potential treatment strategy for propionic acidemia, not only for patients with pseudoexon activation but also for patients with missense variants that have some residual activity of the enzyme.

RESULTS

The pathogenic *PCCA* pseudoexon-activating variation disrupts an hnRNP A1-binding splicing silencer element and simultaneously creates a splicing enhancer element

We first investigated the mechanism of activation and regulation of pseudoexon splicing to identify potential sites that can be targeted to block the inclusion of the *PCCA* pseudoexon using SSOs. As opposed to targeting the pseudoexon splice sites,²⁰ which harbor positions conserved in splice site consensus sequences, targeting SREs

are expected to be more specific, with a lower risk of off-target effects due to the diversity and context dependence of these sequence elements.²⁴ The *PCCA* c.1285-1416A>G variation has been suggested to activate the pseudoexon by the creation of an exonic splicing enhancer (ESE).²⁰ However, we noted that the pseudoexon-activating variation also disrupts a potential hnRNP A1 core UAG/CAG motif,^{25–27} which is supported by *in silico* predictions (Figures S1 and S2).^{28–30} This is also consistent with the observation that the pseudoexon region is covered by enhanced cross-linking and immunoprecipitation (eCLIP) reads from an hnRNP A1 targeted experiment in HepG2 cells (Figure S3).^{31,32} We therefore speculated that the disease-causing variation also disrupts an hnRNP A1-binding exonic splicing silencer (ESS), which normally functions to suppress the pseudoexon. Consequently, this will abolish normal repression and simultaneously allow accessibility of the created ESE, which will further stimulate recognition and splicing of the pseudoexon.

We investigated the functionality of these elements by using the mutagenesis of a *PCCA* pseudoexon splicing reporter minigene (Figure 1A). The *PCCA* c.1285-1416A>G variation (MUT) has previously been demonstrated to cause complete activation in patient fibroblasts,²⁰ and it efficiently activates the pseudoexon in our minigene assay (Figure 1B). An A>T variation (MUT 2) is similarly predicted to disrupt the binding of hnRNP A1, but it is not predicted to create an ESE (Figures S2 and S4). Accordingly, this sequence variation only causes weak activation of the pseudoexon, suggesting that disruption of the hnRNP A1-binding ESS alone is insufficient for complete activation. An A>C variation (MUT 3), also predicted to disrupt the binding of hnRNP A1, is predicted to simultaneously create an ESE and efficiently activates the pseudoexon, indicating that the creation of an ESE is important for complete activation. In addition, two nearby overlapping ESEs are predicted upstream from the *PCCA* c.1285-1416A>G variation. Disruption of the nearest element (MUT 4 + 6) results in lower inclusion levels of the activated pseudoexon, which suggests that this ESE is required for pseudoexon recognition and splicing.

Figure 1. Investigating the mechanism of activation and regulation of the *PCCA* pseudoexon

(A) Schematic representation of the *PCCA* pseudoexon splicing reporter minigene construct and indication of mutagenesis for MUT, MUT 2–6, APOA WT/MUT, and ACADM A/C, C/C, A/T, and C/T variants of the minigene pseudoexon sequence. The minigene construct includes the *PCCA* pseudoexon, flanking introns, and neighboring exons (14 + 15). Location of the *PCCA* c.1285-1416A>G variation is marked in yellow. MaxEnt scores are given for each splice site in the minigene construct. F and R indicate the location of forward and reverse primers for RT-PCR analysis of minigene *PCCA* pseudoexon splicing patterns. ESEs are indicated by green highlights, and hnRNP A1-binding ESSs are indicated by red highlights of the pseudoexon sequence elements. (B) *PCCA* pseudoexon splicing patterns from minigene variants presented in (A) transfected into HepG2 cells. Error bars indicate SEMs, $n = 3$ culture wells. (C) Sequences of 2 sets of biotinylated RNA oligonucleotides covering the splicing regulatory element altered by the *PCCA* c.1285-1416A>G variation used for SPRi (D) and RNA affinity pulldown (E). (D) Binding profiles from SPRi of recombinant hnRNP A1 and hnRNP A2 with protein injections at increasing concentrations. Measurements for hnRNP A1 are fitted to a bimodal 1:2 binding model, and measurements for hnRNP A2 are fitted to a monomodal 1:1 binding model. The equilibrium constant, K_D , is given as an indicator of how well the protein binds at equilibrium. (E) Top splicing factors affected by the *PCCA* c.1285-1416A>G variation (MUT) relative to WT, given by the change in abundance ratio (MUT/WT) from RNA affinity pulldown (members of the hnRNP A/B family are indicated in bold). Splicing factors were included if >2 peptides were detected in all replicates and in both sets of biotinylated RNA oligonucleotides, and if $p < 0.05$ for the change in abundance ratio in at least 2 replicates with applied cutoff values for the abundance ratio, <0.7 and >1.3, reached for at least one of the biotinylated RNA oligonucleotide sets. Error bars indicate SEMs, $n = 3$ from individual experiments. (F) Indication of mutagenesis for M2A1-M5A1 MUT variants of the minigene pseudoexon sequence. Predicted hnRNP A1-binding ESSs are indicated by red highlighting of the pseudoexon sequence elements. M1A1 indicates the element disrupted by the *PCCA* c.1285-1416A>G variation. (G) *PCCA* pseudoexon splicing patterns from minigene variants presented in (F) transfected into HepG2 cells. Error bars indicate SEMs, $n = 3$ culture wells. (H) Endogenous *PCCA* pseudoexon splicing patterns from knockdown of hnRNP A1, hnRNP A2, and both hnRNP A1 and hnRNP A2 in HepG2, HeLa, and HEK293 cells. Error bars indicate SDs, $n = 6$ culture wells from 2 individual experiments (HepG2), $n = 4$ culture wells (HeLa and HEK293). (I) Western blots for validation of hnRNP A1 and hnRNP A2 knockdowns. Ψ , pseudoexon; BGH, bovine growth hormone polyadenylation signal; CMV, cytomegalovirus promoter; KD, knockdown.

To further support the assumption that normal repression of the *PCCA* pseudoexon depends on the presence of an hnRNP A1-binding ESS, and that creation of an ESE is required for complete activation, we replaced the SRE altered by the *PCCA* c.1285-1416A>G variation with similar previously described elements from other genomic contexts (Figures 1A and 1B). The WT sequence from *APOA2* (NM_001643) exon 3 (*APOA* WT) contains an ESE that binds SRSF1 and SRSF2³³ and efficiently activates the *PCCA* pseudoexon. We can disrupt this element (*APOA* MUT) and simultaneously create a putative hnRNP A1-binding ESS (Figures S3 and S4), illustrating the reverse change in regulation that functions to repress the pseudoexon. The WT sequence from *ACADM* (NM_000016) exon 5 (*ACADM* A/C) contains an SRSF1-binding ESE and an hnRNP A1-binding ESS affected by the c.351A>C and c.362C>T variants.^{34,35} The presence of both elements causes weak activation of the *PCCA* pseudoexon, demonstrating that the creation of an ESE alone is insufficient for complete activation in the presence of an antagonizing hnRNP A1-binding ESS. When the ESS is disrupted (*ACADM* C/C), the pseudoexon is efficiently activated, and when the ESE is disrupted (*ACADM* A/T), repression of the pseudoexon is restored. When both elements are disrupted, the pseudoexon is mildly activated, again demonstrating its dependence on an ESS for normal repression. To demonstrate that the observed effects from changing these elements are general and not minigene specific, we replicated this experiment using a different splicing reporter and obtained identical splicing patterns (Figure S5).

We then used biotinylated oligonucleotides covering the SRE affected by the *PCCA* c.1285-1416A>G variation (Figure 1C) and surface plasmon resonance imaging (SPRi) to demonstrate that the sequence variation causes a decrease in the binding of hnRNP A1 (Figure 1D). We further validated this decrease in the binding of hnRNP A1 (and other members of the hnRNP A/B family) by RNA affinity pulldown with subsequent analysis by mass spectrometry (Figure 1E). As indicated by the eCLIP reads covering the *PCCA* pseudoexon (Figure S3), other putative hnRNP A1-binding ESSs exist across the pseudoexon sequence (M2A1–M5A1) (Figure 1F). We investigated the functionality of these elements through inactivation by A>C mutations of the second nucleotides in the core UAG/CAG motifs, which we have previously demonstrated can abolish the binding of hnRNP A1.^{25,34–38} Apart from M5A1, disruption of the putative hnRNP A1-binding ESSs is also consistent with *in silico* predictions (Figure S6). The decrease in the binding of hnRNP A1 to the mutated M4A1 and M3A1+M4A1 elements was demonstrated by RNA affinity pulldown with subsequent analysis by western blotting (Figure S7). Accordingly, the pseudoexon can be mildly activated from the disruption of M2A1, M3A1, or M4A1 in our minigene assay (Figure 1G). These elements likely cooperate with M1A1 in normal repression of the pseudoexon, allowing effective binding of hnRNP A1 and cross-talk between the two regions of ESSs (M1A1+M2A1 and M3A1+M3A4), which is weakened when M1A1 is disrupted by the *PCCA* c.1285-1416A>G variation and antagonized by the binding of serine/arginine-rich (SR) proteins to the newly created ESE that altogether causes complete activation of the pseudoexon.^{39,40} Small

interfering RNA (siRNA)-mediated hnRNP A1 knockdown further supports dependence on hnRNP A1 in the normal repression of the pseudoexon because this results in increased inclusion levels from endogenous *PCCA* (Figures 1H and 1I). Both hnRNP A1 and hnRNP A2 are knocked down to circumvent possible effects from their compensatory relationship.⁴¹

A seemingly benign SNP can activate the *PCCA* pseudoexon and may be a genetic determinant affecting *PCCA* gene expression

Because our results demonstrate that inclusion of the *PCCA* pseudoexon depends on a balance between several SREs and show that the pseudoexon can be activated from multiple sites, we investigated whether SNPs could play a role in *PCCA* expression by affecting pseudoexon inclusion (Figure 2A). Interestingly, SNP 1 increases the pseudoexon inclusion level to 21% (Figure 2B). According to the Hardy-Weinberg equilibrium, this seemingly benign SNP has an estimated carrier frequency of ~1/200 in the African/African American population (rs186983584; C: 0.002655; gnomAD version 3.1.2: <https://gnomad.broadinstitute.org/>), and may thus be a rare but not negligible cause of decreased *PCCA* activity when found in a homozygous or compound heterozygous form.

SNP 3 also causes low-level activation of the pseudoexon, whereas repression is reinforced by the presence of SNP 4 and 6–10. SNP 1 and 3 probably activate the pseudoexon by strengthening the polypyrimidine tract, and accordingly, SNP 3 increases the maximum entropy (MaxEnt) score of the 3' ss from 6.03 to 7.27. The nonactivated WT *PCCA* pseudoexon carries functional splice sites and is on the edge of increased inclusion levels.⁷ Normal repression can be abolished by changes in the balanced regulation of splicing or by small optimizations of the pseudoexon splice sites, and we demonstrate that by introducing only a small increase in the strength of the 5' ss (MaxEnt score increased from 9.77 to 10.47), we induce complete activation of the WT pseudoexon (Figure 2C). Note that none of the cell lines used in the experiments in this study harbor any of the investigated SNP variants.

Targeted SSOs can block inclusion of the *PCCA* pseudoexon to increase both *PCCA* and *PCCB* protein levels and rescue *PCC* enzyme activity in a cellular model

Using our *PCCA* pseudoexon splicing reporter minigene, we performed an SSO walk across the splicing regulatory region altered by the *PCCA* c.1285-1416A>G variation (Figure 3A). We identified SSOs that can restore WT splicing patterns from the mutant minigene and block low-level pseudoexon inclusion from the WT (Figure 3B). Consistent with our minigene results, the most efficient SSOs (SSO 1–3) also cover the upstream functional ESE, and because the SSOs can block pseudoexon inclusion from the WT minigene, this indicates that they cover a region with overall splicing stimulatory activity, even with the presence of the hnRNP A1-binding ESS. This region was also particularly responsive when targeted by some of the 18-mer 2'-O-methoxyethyl/phosphorothioate SSOs from an extensive SSO walk across the WT *PCCA* pseudoexon performed by Lim et al.⁴²

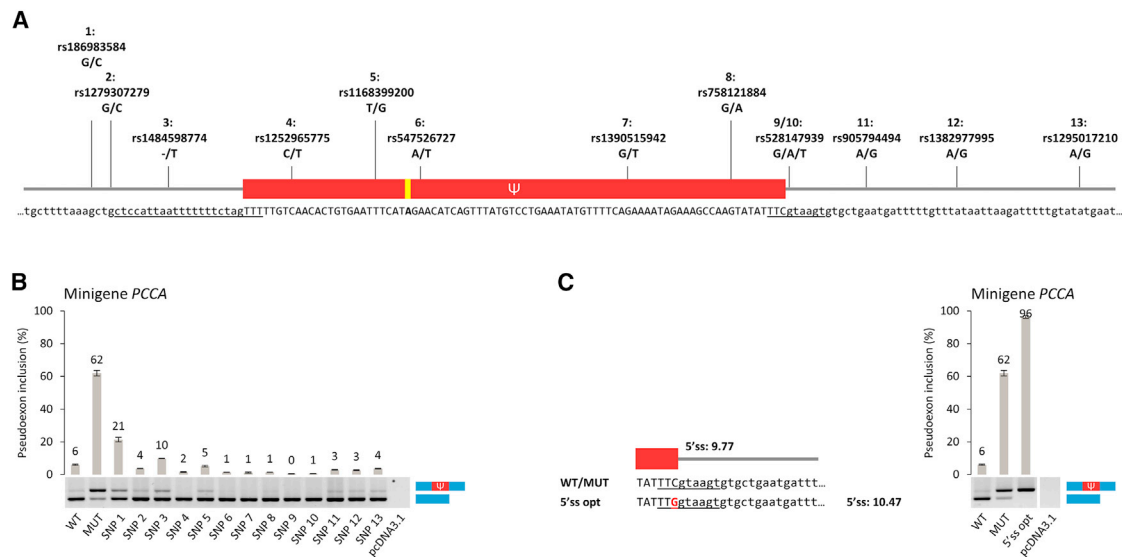


Figure 2. Investigating the landscape of sequence variation around the PCCA pseudoexon

(A) Schematic representation and location of SNP 1–13 introduced to the *PCCA* pseudoexon splicing reporter minigene. The 23-mer 3' splice site and 9-mer 5' splice site sequences for estimation of the MaxEnt scores are underscored. (B) *PCCA* pseudoexon splicing patterns from WT, MUT, and SNP 1–13 minigene variants transfected into HepG2 cells. Error bars indicate SEMs, $n = 3$ culture wells. (C) Indication of mutagenesis for the 5'ss opt variant of the minigene pseudoexon 5' splice site (5'ss) sequence and *PCCA* pseudoexon splicing patterns from WT, MUT, and 5'ss opt minigene variants transfected into HepG2 cells. Error bars indicate SEMs, $n = 3$ culture wells. The MaxEnt score is given for the WT and optimized 5'ss.

We generated an isogenic cellular model of the *PCCA* pseudoexon activation event by using CRISPR gene editing to introduce the pathogenic pseudoexon-activating variation in HepG2 cells, which is a relevant cell line to study because the disease mainly manifests in the liver (Figure 4A). The new cell line is functionally hemizygous for the *PCCA* c.1285-1416A>G variation (HepG2 *PCCA* MUT) because the other allele carries a large complex deletion including exons 13 and 14 (Figure S8), and in-frame deletion of these exons has previously been identified to cause propionic acidemia.⁴³ In addition, we generated a cell line that is homozygous for a 7-bp deletion, c.1285-1411delTAGAACA, exactly covering the hnRNP A1-binding ESS (HepG2 *PCCA* Del7).

We performed SSO transfections of the CRISPR-edited HepG2 cells to verify the effect and efficiency by blocking the inclusion of the endogenous *PCCA* pseudoexon and to investigate the possibility of increasing functional gene expression and PCC enzyme activity by targeting only the *PCCA* subunit. Also in this setting, the *PCCA* c.1285-1416A>G variation causes complete activation of the pseudoexon, and the splicing patterns are restored by SSO treatment (Figure 4B). The 7-bp deletion of the hnRNP A1-binding ESS efficiently activates the pseudoexon, but not to the same level of inclusion, again suggesting that disruption of this ESS is insufficient for complete activation without the simultaneous creation of an ESE. Interestingly, SSO treatment causes an increase in both *PCCA* and *PCCB* protein levels in all three cell lines (Figure 4C) and consequently results in a significant increase in PCC activity (Figure 4D).

Relatively high inclusion levels of the nonactivated WT *PCCA* pseudoexon can be observed in HepG2 cells and across a human tissue panel (Figure S9). Treatment of multiple cell lines with an inhibitor of NMD, cycloheximide (CHX), verifies that some of the pseudoexon-containing transcripts are degraded (Figure S10), which implies that the pseudoexon is included at even higher levels than initially observed. Normal inclusion of this nonfunctional pseudoexon suggests that SSO-mediated modulation of the pseudoexon splicing patterns can be used to regulate *PCCA* gene expression, as previously proposed by Lim et al.⁴² Accordingly, we demonstrate that SSO-mediated blocking of the nonactivated WT *PCCA* pseudoexon is reflected by an increase in *PCCA* protein levels. Remarkably, *PCCB* protein levels are also increased by blocking the *PCCA* pseudoexon. Relative to the stoichiometry of the functional heterododecameric PCC enzyme, the *PCCB* subunit is synthesized in excess from stable mRNA, but *PCCB* monomers are unstable and rapidly degraded in the absence of *PCCA*,^{22,23} as illustrated by the decrease in *PCCB* protein levels observed in HepG2 *PCCA* MUT and Del7 cells relative to WT (Figure 4C). By increasing *PCCA* protein levels, excess *PCCB* is rescued from degradation, and the enzyme activity is thereby increased.

Splice-switching antisense oligonucleotide-mediated blocking of the *PCCA* pseudoexon can restore levels of accumulated biomarkers of propionic acidemia in a cellular model

We used RNA sequencing and differential gene expression analysis to study the transcriptomic effects of SSO treatment in our cellular model of *PCCA* pseudoexon activation in propionic acidemia. The

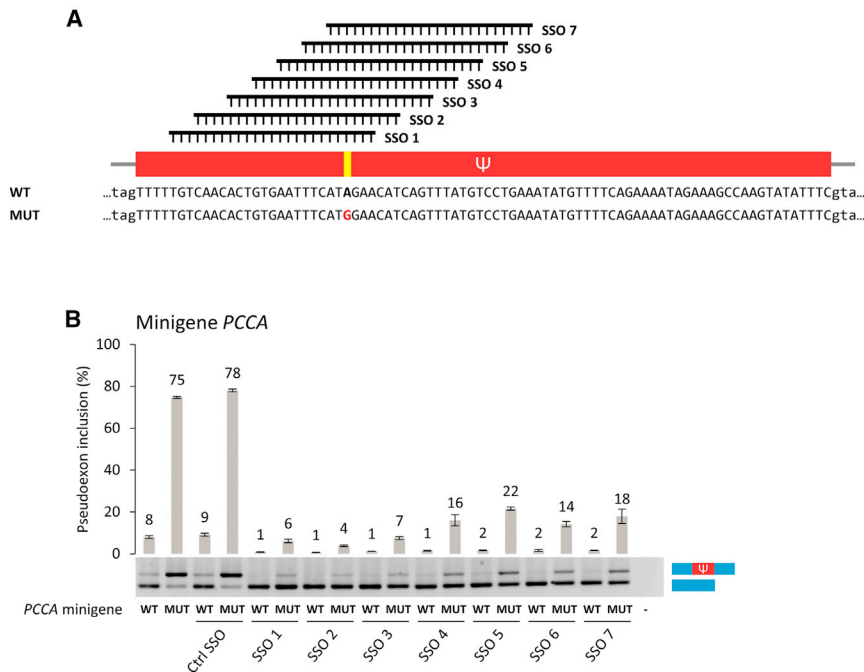


Figure 3. Investigating splice-switching antisense oligonucleotide-mediated modulation of PCCA pseudoexon splicing patterns in minigenes

(A) Schematic representation of the SSO walk with location of SSO 1–7 relative to the PCCA pseudoexon sequence. Location of the PCCA c.1285-1416A>G variation is marked in yellow. (B) PCCA pseudoexon splicing patterns from WT and MUT minigene variants with additional transfection of SSO 1–7 into HepG2 cells. Error bars indicate SEMs, n = 3 culture wells. ctrl, control.

shortening the length of the SSO, which has been demonstrated to significantly reduce SSO off-target activity.⁴⁴ In addition, off-target activity can be reduced by introducing mismatches to the SSO sequence by mixing the SSO chemistry, by combining SSOs targeting the same splicing event, and by SSO delivery through free cellular uptake, which is also more therapeutically relevant.⁴⁴ Because the SSOs used in experiments are complementary to the WT sequence in mutant CRISPR-edited HepG2 cells and complementary to the mutant sequence in control fibroblasts, SSOs with single mismatches can still block the PCCA pseudoexon efficiently.

largest difference between groups is between WT and the two pseudoexon-activating genotypes (Figure 5A), and the direction of change from SSO treatment is similar for all three cell lines. The SSO treatment increases PCCA mRNA levels in all three cell lines, whereas there is no overall effect on the mRNA levels of PCCB (Figure 5B), supporting the idea that the increase in PCCB is post-transcriptional and likely caused at the protein level. By comparing log2 fold changes for genes with a significant differential expression between genotypes—HepG2 PCCA MUT/Del7 versus WT—and between treatment conditions—SSO- versus control-treated HepG2 PCCA MUT/Del7—we observe inverse correlations, indicating some SSO-mediated reversal of transcriptomic effects from PCCA deficiency for the two pseudoexon-activating genotypes (Figure 5C).

We investigated the effect of the SSO treatment on possible hybridization-specific off-targets from the control- and SSO-treated CRISPR-edited HepG2 cells (Figure S11). Sixty-five possible off-targets were identified with NCBI Nucleotide BLAST (<https://blast.ncbi.nlm.nih.gov/Blast.cgi>) of the SSO target sequence (Table S1), from which only one gene (*MIPOL1*) is differentially expressed between treatment conditions. However, no changes in the splicing patterns can be identified as affected by the possible off-target (Figure S12), and the effect on gene expression may thus be secondary to the targeted effect from the SSO. No changes in splicing patterns can be observed from other possible off-targets located within or near exons (Figure S13). Because the SSO efficiently blocks the inclusion of the PCCA pseudoexon with complementarity of just 18 consecutive nucleotides in the HepG2 PCCA Del7 cells, complementarity to *MIPOL1* and other possible off-targets can be reduced by

fibroblasts, SSOs with single mismatches can still block the PCCA pseudoexon efficiently.

Again, using our cellular model, we also investigated the effect of SSO treatment on metabolite profiles (Figure S14). We identify a total of six features with significant differences when comparing the control- and SSO-treated CRISPR-edited HepG2 cells (Figure 5D). The levels of methylcitrate and propionylcarnitine are elevated in PCCA-deficient cells with the pathogenic pseudoexon-activating variation (Figure 5E). These metabolites are also accumulated in propionic acidemia,⁴⁵ which validates the HepG2 PCCA MUT cell line as a cellular model of the disease. Our data show that the accumulated levels of both methylcitrate and propionylcarnitine can be restored by SSO treatment. As expected, the 7-bp deletion does not activate pseudoexon inclusion sufficiently to disrupt protein levels and enzyme activity to a degree that causes elevated levels or accumulation of these biomarkers. The HepG2 PCCA Del7 cell line still possesses ~30% PCC activity relative to WT, whereas no enzyme activity can be measured in HepG2 PCCA MUT without SSO treatment.

Splice-switching antisense oligonucleotide-mediated blocking of the PCCA pseudoexon can increase activity of the heteromeric PCC enzyme in patient fibroblasts with missense variants

To further investigate the therapeutic potential of our most efficient SSO, we investigated the effect on PCC enzyme activity from SSO transfection into control and patient fibroblasts homozygous for the PCCA c.1285-1416A>G variation (Figures 6A and 6B) and into patient fibroblasts with PCCA or PCCB missense variants. Blocking of the activated PCCA pseudoexon results in a significant increase

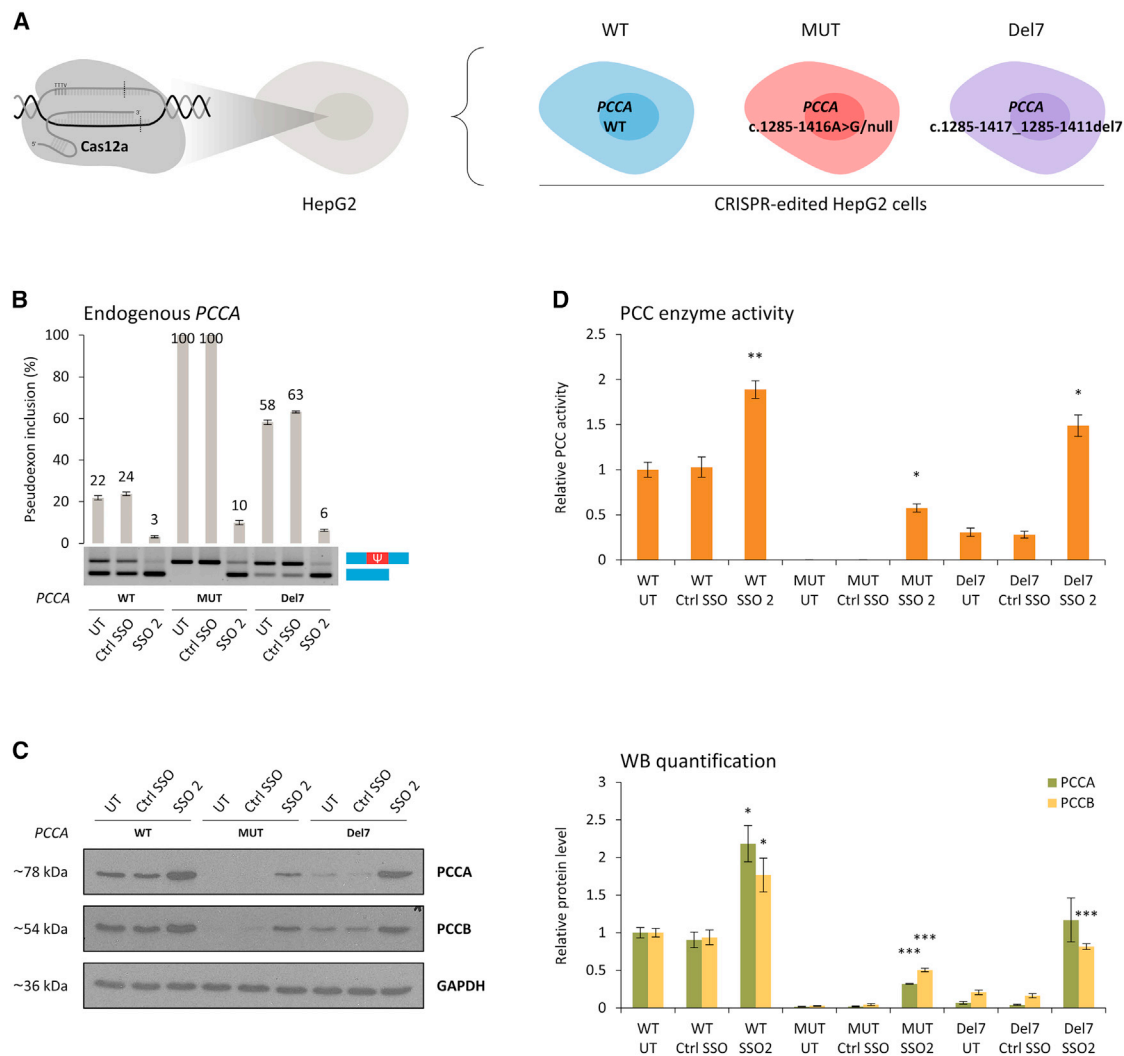


Figure 4. Investigating splice-switching antisense oligonucleotide-mediated modulation of PCCA pseudoexon splicing patterns in a cellular model

(A) Schematic representation of the HepG2 PCCA cell lines generated with CRISPR gene editing. (B) Endogenous PCCA pseudoexon splicing patterns from untransfected (UT), control- and SSO-treated (ctrl SSO and SSO 2) HepG2 PCCA WT (WT), HepG2 PCCA MUT (MUT), and HepG2 PCCA Del7 (Del7) cell lines. Error bars indicate SEMs, $n = 6$ culture wells from 3 individual experiments. (C) Representative western blots from investigation of PCCA and PCCB protein levels between untransfected, control-treated, and SSO-treated HepG2 PCCA cell lines, and protein quantification by densitometry normalized to the immunodetection of GAPDH used as loading control, indicated as the change in protein levels relative to untransfected HepG2 PCCA WT. Comparisons between control- and SSO-treated samples by 2-sample t test in R. * $p < 0.05$; ** $p < 0.005$; *** $p < 0.0005$. Error bars indicate SEMs, $n = 3$ from individual experiments. (D) PCC enzyme activity between untransfected, control-treated, and SSO-treated HepG2 PCCA cell lines, indicated as the change in PCC activity relative to untransfected HepG2 PCCA WT. Comparisons between control- and SSO-treated samples by 2-sample t test in R. * $p < 0.05$; ** $p < 0.005$; *** $p < 0.0005$. Error bars indicate SEMs, $n = 3$ from individual experiments.

from ~5% initial PCC enzyme activity, reaching above the normal activity level relative to control fibroblasts (Figure 6C). Consistent with our observations from WT HepG2 cells, blocking of the nonactivated WT pseudoexon also increases PCC activity in control fibroblasts. This suggests that SSO-mediated blocking of the PCCA pseudoexon can be used as a potential treatment strategy for other PCCA-deficient patients with missense variants that possess some residual enzyme activity, such as PCCA (NM_000282) c.223G>C (p.A75P), c.229C>T (p.R77W), c.412G>A (p.A138T), and c.491T>C (p.I164T).^{14,46}

Transfection of SSOs into patient fibroblasts homozygous for PCCA c.412G>A (p.A138T) and compounds heterozygous for PCCA c.229C>T (p.R77W)/c.1846-2_1852del9 (~3% and ~1% initial activity relative to control fibroblasts) demonstrates a mean 4.5-fold and a mean 10-fold increase in relative PCC activity, respectively, although not statistically significant (Figure 6C).

Moreover, because an increase in PCCA protein levels can stabilize excess PCCB, this further suggests that SSO-mediated blocking of

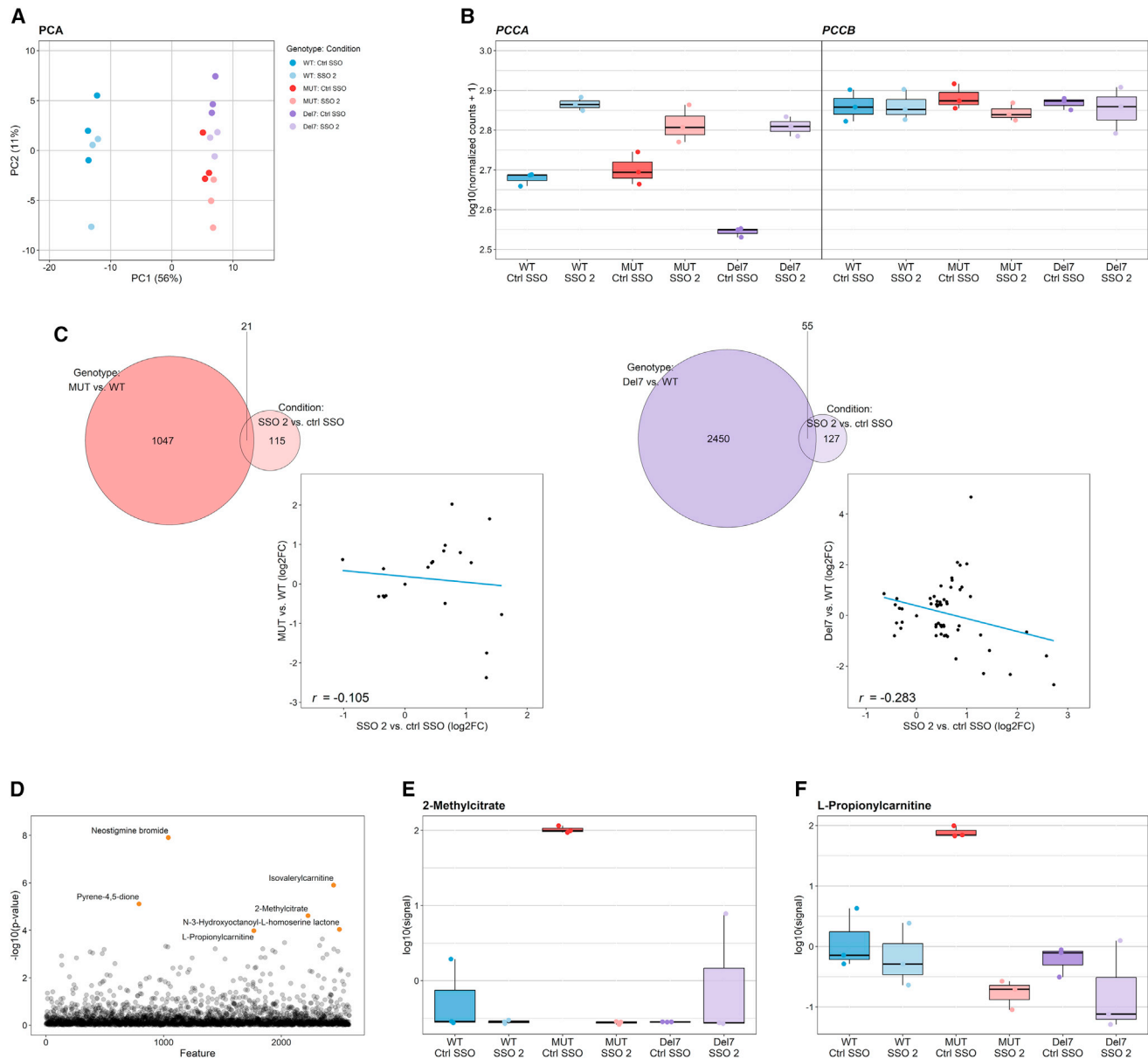


Figure 5. Investigating transcriptomic and metabolomic effects of the pathogenic PCCA pseudoexon activation event and splice-switching antisense oligonucleotide-mediated modulation of pseudoexon splicing patterns

(A) Principal-component analysis (PCA) plot of the variation between control- and SSO-treated (ctrl SSO and SSO 2) HepG2 *PCCA* WT (WT), HepG2 *PCCA* MUT (MUT), and HepG2 *PCCA* Del7 (Del7) cell lines in RNA sequencing data ($n = 3$ from individual experiments). (B) Relative expression of *PCCA* and *PCCB* between control- and SSO-treated HepG2 *PCCA* cell lines indicated as log-transformed normalized read counts from RNA sequencing data. Adjusted p values (p.adj.) from Wald test with post-hoc Benjamini-Hochberg test for differential gene expression between treatment conditions: p.adj. = 1.742×10^{-7} (*PCCA*) and p.adj. = 0.690 (*PCCB*). (C) Venn diagrams with overlap of significant differentially expressed genes (p.adj. < 0.05) and scatterplots comparing the log2 fold changes (log2FC) of the overlapping genes between genotypes; control-treated HepG2 *PCCA* MUT/Del7 versus WT, and between treatment conditions; SSO- versus control-treated HepG2 *PCCA* MUT/Del7. Pearson's correlation, r , is indicated for the overlapping genes in both scatterplots. (D) Scatterplot of 2,578 identified features in metabolomics data ($n = 3$ from individual experiments), indicating features with a significant difference in abundance (orange) between control- and SSO-treated HepG2 *PCCA* cell lines from 1-way ANOVA with post-hoc Fisher's least-significant difference test; p.adj. < 0.05. Significant features: neostigmine bromide (p.adj. = 3.195×10^{-5}), isovalerylcarnitine (p.adj. = 1.609×10^{-3}), pyrene-4,5-dione (p.adj. = 6.627×10^{-3}), 2-methylcitrate (p.adj. = 0.016), L-propionylcarnitine (p.adj. = 0.045), and N-3-hydroxyoctanoyl-L-homoserine lactone (p.adj. = 0.045). PCA plot of the variation between control- and SSO-treated HepG2 *PCCA* cell lines in Figure S14. (E) Relative difference in abundance of 2-methylcitrate between control- and SSO-treated HepG2 *PCCA* cell lines indicated as log-transformed signals from metabolomics data. (F) Relative difference in abundance of L-propionylcarnitine.

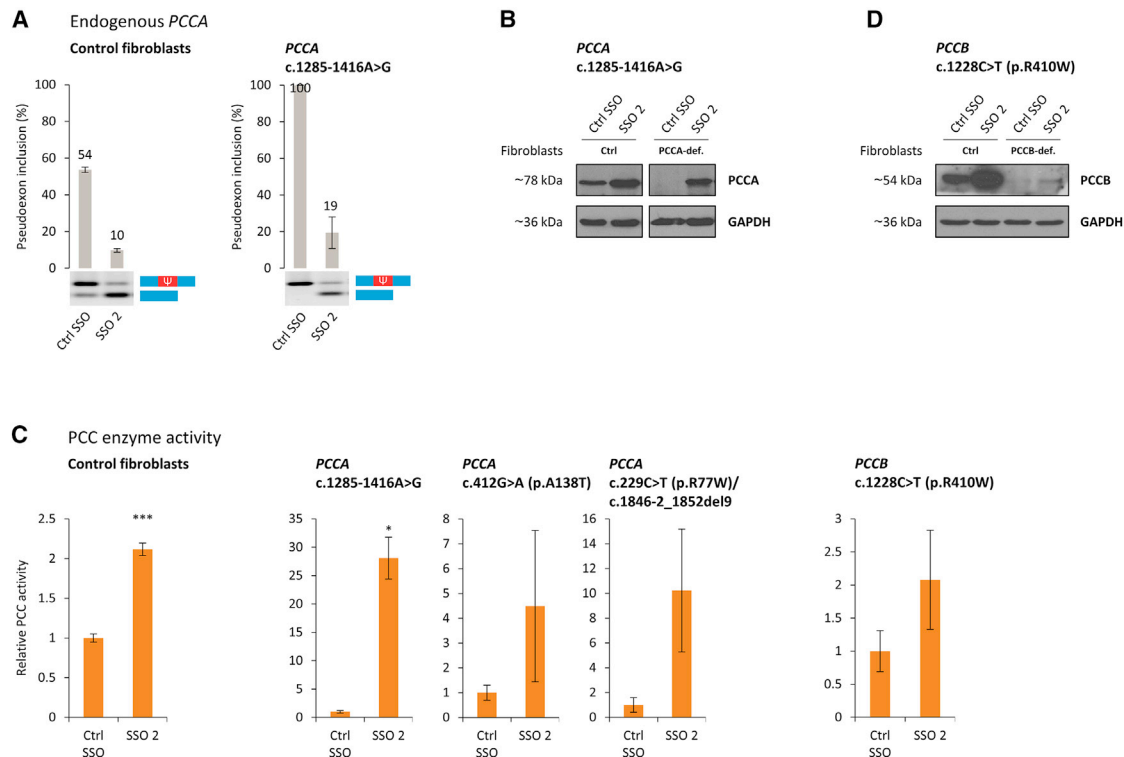


Figure 6. Investigating the therapeutic potential of splice-switching antisense oligonucleotide-mediated modulation of PCCA pseudoexon splicing patterns (A) Endogenous *PCCA* pseudoexon splicing patterns from control- and SSO-treated (ctrl SSO and SSO 2) control fibroblasts and patient fibroblasts homozygous for *PCCA* c.1285-1416A>G. Error bars indicate range, n = 2 culture wells. (B) Representative western blots from investigation of PCCA protein levels between control- and SSO-treated control fibroblasts and patient fibroblasts homozygous for *PCCA* c.1285-1416A>G (*PCCA*-def.). (C) PCC enzyme activity between control- and SSO-treated control fibroblasts, *PCCA*-deficient patient fibroblasts homozygous for *PCCA* c.1285-1416A>G, homozygous for *PCCA* c.412G>A (p.A138T), and compound heterozygous for *PCCA* c.229C>T (p.R77W)/c.1846-2_1852del9, and *PCCB*-deficient patient fibroblasts homozygous for *PCCB* c.1228C>T (p.R410W), indicated as the change in PCC activity relative to control-treated samples. Comparisons by 2-sample t test in R. *p < 0.05; **p < 0.005; ***p < 0.0005. Error bars indicate SEMs, n = 15, 4, 6, 5, and 4, respectively. (D) Representative western blots from investigation of PCCB protein levels between control- and SSO-treated control fibroblasts and patient fibroblasts homozygous for *PCCB* c.1228C>T (*PCCB*-def.).

the *PCCA* pseudoexon can be used as a potential treatment strategy also for *PCCB*-deficient patients with missense variants that possess some residual enzyme activity, such as *PCCB* (NM_000532) c.1228C>T (p.R410W) and c.1606A>G (p.N536D).^{15,47} Transfection of SSOs into patient fibroblasts homozygous for *PCCB* c.1228C>T (p.R410W) (~4% initial activity relative to control fibroblasts) demonstrates a low but detectable increase in PCCB protein levels (Figure 6D) and a mean 2-fold increase in relative PCC activity, although not statistically significant (Figure 6C).

DISCUSSION

The pathogenic *PCCA* c.1285-1416A>G variation is an example of how even a deep-intronic single-nucleotide sequence variation can have dramatic effects on pre-mRNA splicing patterns. The effect of deep-intronic sequence variations that activate pseudoexons by alterations to the splicing regulatory environment is especially difficult to predict and may be overlooked as a cause of disease.⁷ We show that the *PCCA* pseudoexon is activated by the disruption of an hnRNP A1-binding ESS and the simultaneous creation of an

ESE, and this dual change explains the dramatic activation of pseudoexon inclusion. Other putative hnRNP A1-binding ESSs exist across the *PCCA* pseudoexon and may cooperate in the normal repression.^{39,40} Disruption of one ESS is not sufficient to fully activate the pseudoexon, but simultaneous creation of an ESE can antagonize the remaining repression and stimulates complete pseudoexon inclusion. Although the data are consistent across models, it should be noted that the regulation of splicing can be tissue and cell type specific,^{48–50} which can affect the level of pseudoexon inclusion, and we observe that this varies across a human tissue panel (Figure S9).

We demonstrate that the balanced regulation of splicing can be shifted to activate a pseudoexon for inclusion in mRNA from multiple sites, consistent with our findings from investigating the splicing of a *MTRR* pseudoexon.³⁶ Inclusion of the minigene *PCCA* pseudoexon is increased by introducing a seemingly benign SNP, rs186983584 (C). This SNP may be a genetic determinant of a less pronounced pseudoexon activation event that will affect the functional expression of

PCCA. Similarly, other deep-intronic sequence variations have been identified as modifiers of gene expression and possible disease risk factors from disturbing the regulation of splicing that includes the normal repression of cryptic splice sites.^{51–56}

By blocking the inclusion of the *PCCA* pseudoexon using an SSO targeting the splicing regulatory region altered by the pathogenic pseudoexon-activating variation, we can increase the activity of the heterododecameric PCC enzyme by modulating the levels of just one subunit, because the level of *PCCA* is a limiting factor for both PCC subunits. This suggests that the activity of other multisubunit proteins may be increased in a similar way, despite the apparently fixed stoichiometry of the subunits that form the functional protein. It illustrates a principle, in which an increase in the functional mRNA amounts encoding only one subunit is matched by the increased rescue of the other subunit at the protein level. We demonstrate that the PCC enzyme activity can reach the level of controls in patient fibroblasts homozygous for the *PCCA* c.1285-1416A>G variation and ~50% activity relative to WT in the new functionally hemizygous HepG2 *PCCA* MUT cell line, and that this is sufficient to restore the levels of accumulated biomarkers of propionic acidemia. In previous studies, WT PCC activity levels could not be reached from the transfection of a WT *PCCA* expression vector into *PCCA*-deficient patient fibroblasts^{14,57} or from the injection of a *PCCA*-expressing adeno-associated virus vector into the *Pcca*^{−/−} (A138T) mouse model despite elevated levels of *PCCA* protein relative to WT⁵⁸; this was suggested to be due to the imbalanced expression of the two subunits.^{14,58} Accordingly, a much greater increase in PCC enzyme activity has been demonstrated from dual *PCCA* and *PCCB* mRNA transfected into patient fibroblasts at an optimal molar ratio of 1:1, compared to the transfection of single mRNA.⁵⁹ In this study, we demonstrate a significant increase in PCC activity reaching normal levels by SSO treatment in cell lines with *PCCA* pseudoexon activation, and the increase in activity is thereby not limited from the modulation of the endogenous expression.

Splice switching using antisense oligonucleotides has emerged as a promising new strategy in the treatment of genetic diseases,^{60–64} and pseudoexons are optimal targets for SSO treatment, because the generation of WT mRNA transcript will result from blocking pseudoexon inclusion. Other examples of SSO-mediated blocking of an increasing number of disease-associated pseudoexons have been demonstrated to restore enzyme activity.^{20,36,65–67} However, the delivery of antisense oligonucleotide molecules still poses a major challenge and is limited to a few organs, such as liver, kidneys, CNS, and eyes.⁶⁸ The liver would be the main target in the treatment of propionic acidemia. Antisense oligonucleotides will accumulate in liver and kidneys from systemic administration,⁶⁹ and hepatocyte uptake and drug potency can be enhanced through *N*-acetylgalactosamine conjugation targeting the asialoglycoprotein receptor for mediated cellular uptake.^{70,71}

By investigating the mechanism of activation and regulation of the *PCCA* pseudoexon, we have identified an SSO target site from which

pseudoexon inclusion is efficiently blocked. Due to relatively high normal inclusion levels, we demonstrate that the *PCCA* pseudoexon offers an unexploited potential, because SSO-mediated modulation of the WT pseudoexon splicing patterns can regulate *PCCA* gene expression. By modulating the levels of the *PCCA* subunit, excess production of *PCCB* can be rescued from protein degradation to increase PCC enzyme activity. Due to the genetic heterogeneity of propionic acidemia, no clear genotype-phenotype correlations have been discovered in studied patients.^{16–19} Nevertheless, residual PCC enzyme activity appear to determine disease severity, although with notable exceptions.^{16,18} In this study, SSO-mediated blocking of the nonactivated WT *PCCA* pseudoexon results in the increased activity of the heterododecameric PCC enzyme in patient fibroblasts with pathogenic *PCCA* or *PCCB* missense variants, although the overall enzyme activity is still low compared to the relative activity in control fibroblasts. The initial residual enzyme activity and the effect from SSO-mediated blocking of the *PCCA* pseudoexon may be higher in other tissues more relevant to treatment, such as liver, which is the major organ of propionate metabolism and has a higher expression of the PCC subunits. Moreover, it may be possible to alleviate the symptoms of propionic acidemia with just a small increase in PCC enzyme activity. Liver-specific supplementation by the transgenic expression of human *PCCA* resulting in only 10%–20% of WT PCC activity was sufficient to prevent lethal ketoacidosis in early infant periods for the fatal *Pcca*^{−/−} mouse model⁷²; we observed the normalization of metabolites in our HepG2 *PCCA* Del7 cells that had 30% of the control enzyme activity. The SSO-mediated blocking of the nonactivated WT *PCCA* pseudoexon can contribute to alleviate symptoms in both *PCCA*- or *PCCB*-deficient patients with missense or leaky splicing variants^{73,74} that allow for some residual PCC enzyme activity. This represents an example of targeted augmentation of nuclear gene output,⁴² which has shown great potential to increase functional *SCN1A* expression by SSO-mediated blocking of a naturally occurring nonproductive alternative splicing event in the treatment of Dravet syndrome.^{42,75,76} It is plausible that many other pseudoexons can be exploited to regulate gene expression in the treatment of other not only monogenic diseases.

MATERIALS AND METHODS

Cell cultures

HepG2, HeLa, HEK293, and fibroblast cell lines were cultured in RPMI-1640 medium (Sigma-Aldrich, St. Louis, MO) supplemented with 10% fetal bovine serum, l-glutamine (4 mM), and penicillin (100 U/mL)/streptomycin (100 µg/mL) at 37°C in 5% CO₂. We have used four skin fibroblast cell lines derived from propionic acidemia patients with different genotypes: homozygous for *PCCA* c.1285-1416A>G,²⁰ homozygous for *PCCA* c.412G>A (p.A138T),^{46,77} compound heterozygous for *PCCA* c.229C>T (p.R77W)/c.1846-2_1852del9,^{46,77} and homozygous for *PCCB* c.1228C>T (p.R410W) (not previously described). Ethical approval for the present study was granted by the Institutional Ethics Committee of Universidad Autónoma de Madrid (no. UAM CEI 112–2189).

CRISPR gene editing

New HepG2 cell lines HepG2 *PCCA* MUT, HepG2 *PCCA* Del7, and HepG2 *PCCA* WT were generated using the Alt-R CRISPR-Cas12a (Cpf1) system (Integrated DNA Technologies, Coralville, IA) for homology-directed repair. A CRISPR RNA (crRNA) guide sequence with high specificity for the target site was designed using the Breaking-Cas web tool⁷⁸ (<https://bioinfogp.cnb.csic.es/tools/breakingcas>). crRNA (*PCCA*-PE.MUT.crRNA: 5'-UAAUUUCUACUCUUGUAGAUAGGACAUAAACUGAUGUUCUAUG-3') and Cas12a ribonucleoprotein was cotransfected with a 75-nt single-stranded DNA donor template of the *PCCA* c.1285-1416A>G sequence variant (−37/+37 nt) into HepG2 cells at 10 and 3 nM concentrations using Lipofectamine CRISPRMAX Transfection Reagent (Invitrogen, Carlsbad, CA). Cell cultures were expanded from single-cell colonies, and gene editing was confirmed by Sanger sequencing (Figure S8). The HepG2 *PCCA* MUT cell line is functionally hemizygous for the *PCCA* c.1285-1416A>G variation with a large complex deletion on the other allele, spanning from intron 12 to intron 14, including the pseudoexon. The HepG2 *PCCA* Del7 cell line is homozygous for a 7-bp deletion; c.1285-1411delTAGAACA and the HepG2 *PCCA* WT cell line derives from a negative clone in which no *PCCA* gene editing has occurred.

Minigene constructs

The *PCCA* pseudoexon splicing reporter minigenes contain *PCCA* exon 14, intron 14, and exon 15 between *Nhe*I and *Xho*I restriction sites in the pcDNA3.1(+) plasmid vector. Restriction sites *Eco*RI+*Kpn*I and *Bam*HI+*Eco*RI were introduced for easy mutagenesis by insertion of short sequences 98 bp upstream (GAATTCTGGT) and 131 bp downstream (GATCCGAATTC) of the *PCCA* pseudoexon sequence within intron 14. Mutagenesis was performed by Synbio Technologies (Monmouth Junction, NJ), and all of the insert sequences were confirmed by Sanger sequencing.

Transfection of SSOs, siRNA, and minigenes

Cells were grown to or seeded at a density of 60%–80% confluency on the day of transfection. The transfection of SSOs was performed at the time of cell seeding using Lipofectamine RNAiMAX Transfection Reagent (Invitrogen) with final SSO concentrations of 20 nM. All of the SSOs used are RNA oligonucleotides with 2'-*O*-methyl modifications and phosphorothioate backbones (LGC Biosearch Technologies, Riskskov, Denmark) (Table S2). A nontargeting sequence was used as the SSO control. Knockdown was performed by double transfections of ON-TARGETplus SMARTpool siRNA targeting hnRNP A1 (L-008221-00; Dharmacon, Lafayette, CO) and hnRNP A2/B1 (L-011690-01; Dharmacon), using nontargeting siRNA (D-001810-10; Dharmacon) as control. Transfections of siRNA were performed at the time of cell seeding and again after 48 h using Lipofectamine RNAiMAX Transfection Reagent with final siRNA concentrations of 40 nM at both transfections. Plasmid minigenes were transfected 24 h after cell seeding using X-tremeGENE 9 DNA Transfection Reagent (Roche, Mannheim, Germany). HepG2, HeLa, and HEK293 cells were transfected in 12-well plates (3.5 cm²/well) for RNA analysis, in 6-well plates (9.6 cm²/well) for protein analysis, and in

10-cm dishes (56.7 cm²) for metabolite analysis. Fibroblasts were transfected in 6-well plates (9.6 cm²/well) for both RNA and protein analysis. Cells were washed in PBS and harvested for RNA analysis 48 h after SSO transfections, 72 h after the first siRNA transfections, and 48 h after minigene transfections, with no additional SSO or siRNA transfections. Cells were harvested for protein analysis 72 h after SSO transfections and the first siRNA transfections. For cells treated with CHX, the media was changed and replaced with new media containing 40 µg/mL CHX 6 h before cell harvest.

RNA analysis by RT-PCR

Cell lysis was performed by adding TRIzol Reagent (Ambion, Carlsbad, CA). After homogenization of the cell lysates, total RNA was extracted by phase separation with chloroform and precipitation in isopropanol. cDNA was synthesized from 0.5 µg RNA using the High-Capacity cDNA Reverse Transcription Kit (Applied Biosystems, Foster City, CA) in 10-µL reactions. To investigate splicing patterns of the minigene *PCCA* pseudoexon, the region from *PCCA* exon 14 to the bovine growth hormone (BGH) termination sequence of the pcDNA3.1(+) backbone was amplified (*PCCA*.ex14.F: 5'-ACCCCTACAAGTCTTTTGGTTTAC-3' and BGH.R: 5'-AACTAGAAGGCACAGTCGAGGCTG-3') from 1 µL cDNA using TEMPase Hot Start 2× Master Mix (Ampliqon, Odense M, Denmark) in 10-µL PCR reactions. To investigate the splicing patterns of the endogenous *PCCA* pseudoexon, the region from *PCCA* exon 14 to exon 15 was amplified (*PCCA*.ex14.F and *PCCA*.ex15.R: 5'-TTCCTGGTTGGATGCCACTG-3'). (PCR program: 95°C for 15 min, 30 cycles at 95°C for 30 s, 60°C (minigene)/51°C (endogenous) for 30 s, and 72°C for 20 s, followed by 72°C for 5 min.) PCR samples were visualized on 1.5% SeaKem LE agarose (Lonza, Rockland, ME) gels containing 0.5× GelRed (Biotium, Fremont, CA), and pseudoexon inclusion was quantified from molar ratios between PCR products using the Fragment Analyzer system (Advanced Analytical Technologies, Ames, IA).

Protein analysis by western blotting

Cells were disrupted by freeze-thawing in lysis buffer (10 mM Tris-HCl pH 7.5, 150 mM NaCl, 0.1% Triton X-100, 10% glycerol) with protease inhibitor and centrifuged for 10 min at 4°C. The supernatant was collected, and the protein concentration was determined by the Bradford method (Bio-Rad, Hercules, CA). Equal amounts of lysed extracts were loaded on a 10% SDS-polyacrylamide gel. After electrophoresis, proteins were transferred to a nitrocellulose membrane (iBlot 2 Transfer Stacks, mini) in an iBlot 2 Gel Transfer Device (Invitrogen). Immunodetection was carried out using commercially available primary antibodies against *PCCA* (1:500; sc-374341; Santa Cruz Biotechnology, Santa Cruz, CA) or *PCCB* (1:500; sc-393929; Santa Cruz Biotechnology), and glyceraldehyde 3-phosphate dehydrogenase (GAPDH) (1:5,000; ab8245; Abcam; Cambridge, UK) as loading control, with a secondary antibody against mouse immunoglobulin G (IgG) (1:2,000; no. 7076; Cell Signaling Technology, Danvers, MA). Antibody binding was detected by enhanced chemiluminescence (GE Healthcare, Buckinghamshire, UK). Protein

quantification was performed using a GS-900 Calibrated Densitometer (Bio-Rad).

For siRNA knockdown experiments, cell lysis was performed by adding M-PER lysis buffer (Thermo Scientific, Rockford, IL) supplemented with 1× cOmplete Protease Inhibitor Cocktail (Roche) and 1 mM PMSF. Protein concentration was estimated using the Pierce BCA Protein Assay Kit (Thermo Scientific). Equal amounts of lysed extracts were loaded on a NuPAGE 4–12% Bis-Tris Gel (Invitrogen) and transferred to a polyvinylidene fluoride membrane. Immunodetection was carried out using primary antibodies against hnRNP A1 (1:1,000; R9778; Sigma-Aldrich) or hnRNP A2/B1 (1:1,000; sc-53531; Santa Cruz Biotechnology), and HPRT1 (1:1,000; HPA006360; Sigma-Aldrich) as loading control.

PCC enzyme activity assay

PCC activity was assayed by measuring the enzyme-dependent incorporation of ^{14}C -bicarbonate into nonvolatile products from the Krebs cycle, as previously described.⁷⁹ Briefly, cells were resuspended in 20 mM Tris-HCl pH 8.0 with 0.81 mM glutathione and disrupted by freeze-thaw cycles. The enzymatic reaction was initiated with the addition of the homogenate, maintained at 30°C for 20 min, and stopped with 30% trichloroacetic acid. The samples were centrifuged at $16,873 \times g$ for 15 min, the supernatant was transferred to a scintillation vial, and subjected to an evaporation process at room temperature for 24–48 h. The nonvolatile products were measured in a Tri-Carb 2810 TR Liquid Scintillation Counter (PerkinElmer, Waltham, MA) after 48 h. PCC activity is expressed in picomoles of incorporated ^{14}C min^{−1} mg^{−1} of total protein.

RNA affinity pulldown and protein quantification by mass spectrometry

Two sets of 3'-end biotinylated RNA oligonucleotides (LGC Biosearch Technologies) (Table S3) covering the same region of the PCCA pseudoexon were used to perform affinity purification of RNA-binding proteins as previously described.³⁵ A total of 1,000 pmol of each 3' end biotin-coupled RNA oligonucleotide were immobilized in 50 μL streptavidin-coupled magnetic beads (Dynabeads M-280 Streptavidin; Invitrogen) and incubated with HeLa nuclear extract (CILBiotech, Mons, Belgium). Tandem Mass Tag 6-plex labeling of eluted RNA-binding proteins was performed using the TMTsixplex Isobaric Mass Tagging Kit (Thermo Scientific) and analysis by liquid chromatography-tandem mass spectrometry (LC-MS/MS) was performed as previously described.⁸⁰

Or proteins were eluted in XT sample buffer (Bio-Rad) and analyzed by western blotting with immunodetection using primary antibodies against hnRNP A1 (1:2,000; R9778; Sigma-Aldrich), hnRNP A2/B1 (1:1,000; sc-53531; Santa Cruz Biotechnology), TDP-43 (1:1,000; 10782-2-AP; Proteintech, Rosemont, IL), and hnRNP K (1:1,000; sc-28380; Santa Cruz Biotechnology).

SPRi

SPRi was carried out as previously described.⁸⁰ Briefly, biotinylated RNA oligonucleotides (LGC Biosearch Technologies) (Table S3) were immobilized onto a G-streptococcus sensor chip (Ssens, Enschede, the Netherlands) for 20 min. The following recombinant proteins were injected for 10 min, followed by dissociation for 8 min: 6.25–200 nM hnRNP A1 (TP303314; OriGene Technologies, Rockville, MD) and 6.25–100 nM hnRNP A2 (TP319318; OriGene Technologies). A continuous flow of SPR buffer (10 mM Tris-HCl, pH 7.9, 150 mM KCl, 3.4 mM EDTA, 0.005% Tween 20) was injected both before, during, and after protein injections. Nuclear extract was used as a control for the binding efficiency of oligonucleotides. Binding hnRNP A2 was fitted to a 1:1 kinetics model with Scrubber2 (version 2.1.1.0, BioLogics). For hnRNP A1, a biphasic 1:2 model was used in ClampXP (version 3.50, Biosensor Data Analysis).

RNA sequencing and analysis

cDNA libraries were prepared from 500 ng RNA using the NEBNext Ultra II Directional RNA Library Prep Kit (New England Biolabs, Ipswich, MA) with rRNA depletion. Libraries were quantified by qPCR using the Kapa Library Quantification Kit (Roche), and the pooled library (from 27 RNA samples) was loaded to an SP flow cell and sequenced on the NovaSeq 6000 platform (Illumina, San Diego, CA) with 2×150 -bp paired-end sequencing. RNA sequencing reads were mapped to the GRCh38 reference genome using STAR (version 2.6.1a).⁸¹ Differential gene expression analysis was performed with DESeq2,⁸² using read counts overlapping genes of the Ensembl (release 93)⁸³ annotation reference.

Metabolite extraction and metabolomics

Cells were washed twice in cold 10 mM ammonium acetate, scraped off the culture dish, pelleted, and frozen at -80°C before metabolite extraction. Ice-cold extraction solvent, 1 mL (50% methanol, 30% acetonitrile, 20% water), was added to the cell pellets. The mixture was agitated at 1,000 rpm for 10 min at 4°C . The extracts were subsequently centrifuged ($16,000 \times g$, 4°C , 15 min). The supernatants were collected and transferred to new tubes, lyophilized, and stored at -20°C until further analysis. The samples were resuspended in 30 μL 0.1% formic acid, 8 μL of which were transferred to a pooled sample for quality control (QC). A total of 5 μL was injected using Vanquish Horizon UPLC (ultraperformance liquid chromatography; Thermo Fisher Scientific, Waltham, MA), and compounds were separated on a Zorbax Eclipse Plus C18 guard (2.1×50 mm and 1.8 μm particle size; Agilent Technologies, Santa Clara, CA) and an analytical column (2.1×150 mm and 1.8 μm particle size; Agilent Technologies) kept at 40°C . The analytes were eluted using a flow rate of 400 $\mu\text{L}/\text{min}$ and the following composition of eluent A (0.1% formic acid) and eluent B (0.1% formic acid; acetonitrile) solvents: 3% B from 0 to 1.5 min, 3%–40% B from 1.5 to 4.5 min, 40%–95% B from 4.5 to 7.5 min, 95% B from 7.5 to 10.1 min, and 95%–3% B from 10.1 to 10.5 min, before equilibration for 3.5 min with the initial conditions. The flow from the UPLC was coupled to a Q Exactive HF mass spectrometer (Thermo Fisher Scientific) for mass spectrometric analysis in both positive and negative ion mode.

Raw data were processed with MzMine⁸⁴ (version 2.53). Compounds were annotated at metabolomics standards initiative⁸⁵ level 2 using local MS/MS spectra databases of the National Institute of Standards and Technology 17 and the MassBank of North America. The datasets were corrected for signal drift using the R package statTarget.⁸⁶ Finally, data were normalized using QC group, log transformation (base 10), and auto scaling, all done in MetaboAnalyst⁸⁷ (<https://www.metaboanalyst.ca/>).

In silico predictions

Changes in SRE activities were predicted using HEXplorer²⁸ (https://www2.hhu.de/rna/html/hexplorer_score.php) and HExoSplice²⁹ (<http://bioinfo.univ-rouen.fr/HExoSplice/inputs.php>). Location of and changes in SR protein binding motifs were predicted using ESEfinder 3.0^{88,89} (<http://krainer01.cshl.edu/cgi-bin/tools/ESE3/esefinder.cgi?process=home>) with default threshold values, and changes in putative hnRNP A1 binding motifs were predicted using DeepCLIP³⁰ (<https://deepclip-web.compbio.sdu.dk/>) with the HNRNP A1_BRUUN pretrained model. Splice site scores were estimated as the MaxEnt score using MaxEntScan⁹⁰ (http://genes.mit.edu/burgelab/maxent/Xmaxentscan_scoreseq.html).

DATA AND CODE AVAILABILITY

All of the relevant data supporting the findings of this study are presented in the article or in the supplemental material. Raw data from RNA sequencing are deposited in ArrayExpress (<https://www.ebi.ac.uk/biostudies/arrayexpress>); E-MTAB-13549, and metabolomics data are deposited in Figshare (<https://figshare.com/>; <https://doi.org/10.6084/m9.figshare.24541357.v1>). Additional information and other raw data are available from the corresponding author upon reasonable request.

SUPPLEMENTAL INFORMATION

Supplemental information can be found online at <https://doi.org/10.1016/j.omtn.2023.102101>.

ACKNOWLEDGMENTS

We thank Professor Magdalena Ugarte for the use of patient-derived fibroblasts from the collection at CEDEM (Centro de Diagnostico de Enfermedades Moleculares). We thank Aristides López-Márquez for help with the CRISPR gene editing design and protocol. We thank Asbjørn Kofoed Seide, Anne Sofie Eybye Nielsen, Michael Silva, and Stefanie Bundgaard Flyvbjerg for technical support.

This work was supported by grants to B.S.A. from the Danish Medical Research Council (no. 9039-00281B) and the Novo Nordisk Foundation (NNF 19OC0058588), and by grants to L.R.D.: Grant PID2019-105344RB-I00/AEI/10.13039/501100011033 from the Spanish Ministry of Science and Innovation and the European Regional Development Fund, and grant XX National Call 2020 from Fundación Ramón Areces. The work was performed in Odense, Denmark, and in Madrid, Spain.

AUTHOR CONTRIBUTIONS

B.S.A. conceptualized this study. U.S.S.P. and M.D. performed the minigene experiments. L.L.H. performed SPRI. M.D. and U.S.S.P. performed RNA affinity pulldown. M.R.L. performed LC-MS/MS protein quantification. M.D. performed hnRNP A1/A2 knockdown. U.S.S.P. performed CRISPR gene editing, SSO transfections of CRISPR-edited HepG2 cells, and, with supervision from T.K.D., RNA sequencing and analysis. J.F.H. performed metabolomics. A.M.-P. and M.D. performed SSO transfections of patient-derived fibroblasts. A.M.-P. performed PCCA/PCCB western blot analyses and PCC enzyme activity assays. B.S.A., L.R.D., E.R., and N.J.F. provided supervision. U.S.S.P., M.D., and B.S.A. drafted and revised the manuscript. All of the authors reviewed the final draft.

DECLARATION OF INTERESTS

The authors declare no competing interests.

REFERENCES

- Baralle, M., and Baralle, F.E. (2018). The splicing code. *Biosystems* 164, 39–48.
- Wang, Z., Rolish, M.E., Yeo, G., Tung, V., Mawson, M., and Burge, C.B. (2004). Systematic Identification and Analysis of Exonic Splicing Silencers. *Cell* 119, 831–845.
- Wahl, M.C., Will, C.L., and Lührmann, R. (2009). The Spliceosome: Design Principles of a Dynamic RNP Machine. *Cell* 136, 701–718.
- Wang, Z., and Burge, C.B. (2008). Splicing regulation: From a parts list of regulatory elements to an integrated splicing code. *RNA* 14, 802–813.
- Graveley, B.R. (2000). Sorting out the complexity of SR protein functions. *RNA* 6, 1197–1211.
- Scotti, M.M., and Swanson, M.S. (2016). RNA mis-splicing in disease. *Nat. Rev. Genet.* 17, 19–32.
- Petersen, U.S.S., Doktor, T.K., and Andresen, B.S. (2022). Pseudoexon activation in disease by non-splice site deep intronic sequence variation - wild type pseudoexons constitute high-risk sites in the human genome. *Hum. Mutat.* 43, 103–127.
- Vaz-Drago, R., Custódio, N., and Carmo-Fonseca, M. (2017). Deep intronic mutations and human disease. *Hum. Genet.* 136, 1093–1111.
- Dhir, A., and Buratti, E. (2010). Alternative splicing: role of pseudoexons in human disease and potential therapeutic strategies. *FEBS J.* 277, 841–855.
- Lykke-Andersen, S., and Jensen, T.H. (2015). Nonsense-mediated mRNA decay: an intricate machinery that shapes transcriptomes. *Nat. Rev. Mol. Cell Biol.* 16, 665–677.
- Haijes, H.A., Jans, J.J.M., Tas, S.Y., Verhoeven-Duif, N.M., and van Hasselt, P.M. (2019). Pathophysiology of propionic and methylmalonic acidemias. Part 1: Complications. *J. Inherit. Metab. Dis.* 42, 730–744.
- Haijes, H.A., van Hasselt, P.M., Jans, J.J.M., and Verhoeven-Duif, N.M. (2019). Pathophysiology of propionic and methylmalonic acidemias. Part 2: Treatment strategies. *J. Inherit. Metab. Dis.* 42, 745–761.
- Wongkittichote, P., Ah Mew, N., and Chapman, K.A. (2017). Propionyl-CoA carboxylase - A review. *Mol. Genet. Metabol.* 122, 145–152.
- Clavero, S., Martínez, M.A., Pérez, B., Pérez-Cerdá, C., Ugarte, M., and Desviat, L.R. (2002). Functional characterization of PCCA mutations causing propionic acidemia. *Biochim. Biophys. Acta* 1588, 119–125.
- Pérez-Cerdá, C., Clavero, S., Pérez, B., Rodríguez-Pombo, P., Desviat, L.R., and Ugarte, M. (2003). Functional analysis of PCCB mutations causing propionic acidemia based on expression studies in deficient human skin fibroblasts. *Biochim. Biophys. Acta* 1638, 43–49.
- Desviat, L.R., Pérez, B., Pérez-Cerdá, C., Rodríguez-Pombo, P., Clavero, S., and Ugarte, M. (2004). Propionic acidemia: mutation update and functional and structural effects of the variant alleles. *Mol. Genet. Metabol.* 83, 28–37.

17. Kraus, J.P., Spector, E., Venezia, S., Estes, P., Chiang, P.W., Creadon-Swindell, G., Müllerleile, S., de Silva, L., Barth, M., Walter, M., et al. (2012). Mutation analysis in 54 propionic acidemia patients. *J. Inher. Metab. Dis.* 35, 51–63.
18. Rivera-Barahona, A., Navarrete, R., García-Rodríguez, R., Richard, E., Ugarte, M., Pérez-Cerdá, C., Pérez, B., Gámez, A., and Desviat, L.R. (2018). Identification of 34 novel mutations in propionic acidemia: Functional characterization of missense variants and phenotype associations. *Mol. Genet. Metabol.* 125, 266–275.
19. Liu, Y., Chen, Z., Dong, H., Ding, Y., He, R., Kang, L., Li, D., Shen, M., Jin, Y., Zhang, Y., et al. (2022). Analysis of the relationship between phenotypes and genotypes in 60 Chinese patients with propionic acidemia: a fourteen-year experience at a tertiary hospital. *Orphanet J. Rare Dis.* 17, 135.
20. Rincón, A., Aguado, C., Desviat, L.R., Sánchez-Alcudia, R., Ugarte, M., and Pérez, B. (2007). Propionic and Methylmalonic Acidemia: Antisense Therapeutics for Intronic Variations Causing Aberrantly Spliced Messenger RNA. *Am. J. Hum. Genet.* 81, 1262–1270.
21. Campeau, E., Dupuis, L., Leclerc, D., and Gravel, R.A. (1999). Detection of a Normally Rare Transcript in Propionic Acidemia Patients with mRNA Destabilizing Mutations in the PCCA Gene. *Hum. Mol. Genet.* 8, 107–113.
22. Lamhonwah, A.M., and Gravel, R.A. (1987). Propionicacidemia: absence of alpha-chain mRNA in fibroblasts from patients of the pccA complementation group. *Am. J. Hum. Genet.* 41, 1124–1131.
23. Ohura, T., Kraus, J.P., and Rosenberg, L.E. (1989). Unequal synthesis and differential degradation of propionyl CoA carboxylase subunits in cells from normal and propionic acidemia patients. *Am. J. Hum. Genet.* 45, 33–40.
24. Fu, X.D., and Ares, M., Jr. (2014). Context-dependent control of alternative splicing by RNA-binding proteins. *Nat. Rev. Genet.* 15, 689–701.
25. Bruun, G.H., Doktor, T.K., Borch-Jensen, J., Masuda, A., Krainer, A.R., Ohno, K., and Andresen, B.S. (2016). Global identification of hnRNP A1 binding sites for SSO-based splicing modulation. *BMC Biol.* 14, 54.
26. Huelga, S.C., Vu, A.Q., Arnold, J.D., Liang, T.Y., Liu, P.P., Yan, B.Y., Donohue, J.P., Shiue, L., Hoon, S., Brenner, S., et al. (2012). Integrative Genome-wide Analysis Reveals Cooperative Regulation of Alternative Splicing by hnRNP Proteins. *Cell Rep.* 1, 167–178.
27. Burd, C.G., and Dreyfuss, G. (1994). RNA binding specificity of hnRNP A1: significance of hnRNP A1 high-affinity binding sites in pre-mRNA splicing. *EMBO J.* 13, 1197–1204.
28. Erkelenz, S., Theiss, S., Otte, M., Widera, M., Peter, J.O., and Schaal, H. (2014). Genomic HEXploring allows landscaping of novel potential splicing regulatory elements. *Nucleic Acids Res.* 42, 10681–10697.
29. Tubeuf, H., Charbonnier, C., Soukarié, O., Blavier, A., Lefebvre, A., Dauchel, H., Frebourg, T., Gaildrat, P., and Martins, A. (2020). Large-scale comparative evaluation of user-friendly tools for predicting variant-induced alterations of splicing regulatory elements. *Hum. Mutat.* 41, 1811–1829.
30. Grønning, A.G.B., Doktor, T.K., Larsen, S.J., Petersen, U.S.S., Holm, L.L., Bruun, G.H., Hansen, M.B., Hartung, A.M., Baumbach, J., and Andresen, B.S. (2020). DeepCLIP: predicting the effect of mutations on protein-RNA binding with deep learning. *Nucleic Acids Res.* 48, 7099–7118.
31. ENCODE Project Consortium (2012). An integrated encyclopedia of DNA elements in the human genome. *Nature* 489, 57–74.
32. Luo, Y., Hitz, B.C., Gabdank, I., Hilton, J.A., Kagda, M.S., Lam, B., Myers, Z., Sud, P., Jou, J., Lin, K., et al. (2020). New developments on the Encyclopedia of DNA Elements (ENCODE) data portal. *Nucleic Acids Res.* 48, D882–D889.
33. Arrisi-Mercado, P., Romano, M., Muro, A.F., and Baralle, F.E. (2004). An Exonic Splicing Enhancer Offsets the Atypical GU-rich 3' Splice Site of Human Apolipoprotein A-II Exon 3. *J. Biol. Chem.* 279, 39331–39339.
34. Nielsen, K.B., Sørensen, S., Cartegni, L., Corydon, T.J., Doktor, T.K., Schroeder, L.D., Reinert, L.S., Elpeleg, O., Krainer, A.R., Gregersen, N., et al. (2007). Seemingly Neutral Polymorphic Variants May Confer Immunity to Splicing-Inactivating Mutations: A Synonymous SNP in Exon 5 of MCAD Protects from Deleterious Mutations in a Flanking Exonic Splicing Enhancer. *Am. J. Hum. Genet.* 80, 416–432.
35. Holm, L.L., Doktor, T.K., Hansen, M.B., Petersen, U.S.S., and Andresen, B.S. (2022). Vulnerable exons, like ACADM exon 5, are highly dependent on maintaining a correct balance between splicing enhancers and silencers. *Hum. Mutat.* 43, 253–265.
36. Palhais, B., Præstegaard, V.S., Sabaratnam, R., Doktor, T.K., Lutz, S., Burda, P., Suormala, T., Baumgartner, M., Fowler, B., Bruun, G.H., et al. (2015). Splice-shifting oligonucleotide (SSO) mediated blocking of an exonic splicing enhancer (ESE) created by the prevalent c.903+469T>C MTRR mutation corrects splicing and restores enzyme activity in patient cells. *Nucleic Acids Res.* 43, 4627–4639.
37. Olsen, R.K.J., Brøner, S., Sabaratnam, R., Doktor, T.K., Andersen, H.S., Bruun, G.H., Gahrn, B., Stenbroen, V., Olpin, S.E., Dobbie, A., et al. (2014). The ETFDH c.158A>G Variation Disrupts the Balanced Interplay of ESE- and ESS-Binding Proteins thereby Causing Missplicing and Multiple Acyl-CoA Dehydrogenation Deficiency. *Hum. Mutat.* 35, 86–95.
38. Doktor, T.K., Schroeder, L.D., Vested, A., Palmfeldt, J., Andersen, H.S., Gregersen, N., and Andresen, B.S. (2011). SMN2 exon 7 splicing is inhibited by binding of hnRNP A1 to a common ESS motif that spans the 3' splice site. *Hum. Mutat.* 32, 220–230.
39. Zhu, J., Mayeda, A., and Krainer, A.R. (2001). Exon Identity Established through Differential Antagonism between Exonic Splicing Silencer-Bound hnRNP A1 and Enhancer-Bound SR Proteins. *Mol. Cell* 8, 1351–1361.
40. Okunola, H.L., and Krainer, A.R. (2009). Cooperative-Binding and Splicing-Repressive Properties of hnRNP A1. *Mol. Cell Biol.* 29, 5620–5631.
41. Hutchison, S., LeBel, C., Blanchette, M., and Chabot, B. (2002). Distinct Sets of Adjacent Heterogeneous Nuclear Ribonucleoprotein (hnRNP) A1/A2 Binding Sites Control 5' Splice Site Selection in the hnRNP A1 mRNA Precursor. *J. Biol. Chem.* 277, 29745–29752.
42. Lim, K.H., Han, Z., Jeon, H.Y., Kach, J., Jing, E., Weyn-Vanhenhenryck, S., Downs, M., Corriero, A., Oh, R., Scharner, J., et al. (2020). Antisense oligonucleotide modulation of non-productive alternative splicing upregulates gene expression. *Nat. Commun.* 11, 3501.
43. Desviat, L.R., Sanchez-Alcudia, R., Pérez, B., Pérez-Cerdá, C., Navarrete, R., Vijzelaar, R., and Ugarte, M. (2009). High frequency of large genomic deletions in the PCCA gene causing propionic acidemia. *Mol. Genet. Metabol.* 96, 171–176.
44. Scharner, J., Ma, W.K., Zhang, Q., Lin, K.T., Rigo, F., Bennett, C.F., and Krainer, A.R. (2020). Hybridization-mediated off-target effects of splice-switching antisense oligonucleotides. *Nucleic Acids Res.* 48, 802–816.
45. Longo, N., Sass, J.O., Jurecka, A., and Vockley, J. (2022). Biomarkers for drug development in propionic and methylmalonic acidemias. *J. Inher. Metab. Dis.* 45, 132–143.
46. Pérez-Cerdá, C., Merinero, B., Rodríguez-Pombo, P., Pérez, B., Desviat, L.R., Muro, S., Richard, E., García, M.J., Gangoiti, J., Ruiz Sala, P., et al. (2000). Potential relationship between genotype and clinical outcome in propionic acidemia patients. *Eur. J. Hum. Genet.* 8, 187–194.
47. Pérez-Cerdá, C., Merinero, B., Martí, M., Cabrera, J.C., Peña, L., García, M.J., Gangoiti, J., Sanz, P., Rodríguez-Pombo, P., Hoenicka, J., et al. (1998). An unusual late-onset case of propionic acidemia: biochemical investigations, neuroradiological findings and mutation analysis. *Eur. J. Pediatr.* 157, 50–52.
48. Wang, E.T., Sandberg, R., Luo, S., Khrebukova, I., Zhang, L., Mayr, C., Kingsmore, S.F., Schroth, G.P., and Burge, C.B. (2008). Alternative isoform regulation in human tissue transcriptomes. *Nature* 456, 470–476.
49. Nilsen, T.W., and Graveley, B.R. (2010). Expansion of the eukaryotic proteome by alternative splicing. *Nature* 463, 457–463.
50. Palhais, B., Dembic, M., Sabaratnam, R., Nielsen, K.S., Doktor, T.K., Bruun, G.H., and Andresen, B.S. (2016). The prevalent deep intronic c. 639+919 G>A GLA mutation causes pseudoxon activation and Fabry disease by abolishing the binding of hnRNP A1 and hnRNP A2/B1 to a splicing silencer. *Mol. Genet. Metabol.* 119, 258–269.
51. Coulombe-Huntington, J., Lam, K.C.L., Dias, C., and Majewski, J. (2009). Fine-Scale Variation and Genetic Determinants of Alternative Splicing across Individuals. *E.T. Dermatzakis, ed.* 5, e1000766.
52. Lalonde, E., Ha, K.C.H., Wang, Z., Bemmo, A., Kleinman, C.L., Kwan, T., Pastinen, T., and Majewski, J. (2011). RNA sequencing reveals the role of splicing polymorphisms in regulating human gene expression. *Genome Res.* 21, 545–554.
53. Vatanavicharn, N., Champattanachai, V., Liammongkolkul, S., Sawangareetrakul, P., Keerachamroen, S., Ketudat Cairns, J.R., Srisomsap, C., Sathienkijkanhai, A.,

- Shotelersuk, V., Kamolsilp, M., et al. (2012). Clinical and molecular findings in Thai patients with isolated methylmalonic acidemia. *Mol. Genet. Metabol.* 106, 424–429.
54. Lenglet, M., Robriquet, F., Schwarz, K., Camps, C., Couturier, A., Hoogewijs, D., Buffet, A., Knight, S.J.L., Gad, S., Couvé, S., et al. (2018). Identification of a new VHL exon and complex splicing alterations in familial erythrocytosis or von Hippel-Lindau disease. *Blood* 132, 469–483.
55. Lee, W., Zernant, J., Nagasaki, T., Molday, L.L., Su, P.Y., Fishman, G.A., Tsang, S.H., Molday, R.S., and Allikmets, R. (2021). Cis-acting modifiers in the ABCA4 locus contribute to the penetrance of the major disease-causing variant in Stargardt disease. *Hum. Mol. Genet.* 30, 1293–1304.
56. Zhang, Z., Blumenfeld, J., Ramnauth, A., Barash, I., Zhou, P., Levine, D., Parker, T., and Rennert, H. (2022). A common intronic single nucleotide variant modifies PKD1 expression level. *Clin. Genet.* 102, 483–493.
57. Rodriguez-Pombo, P., Pérez-Cerdá, C., Desviat, L.R., Pérez, B., Ugarte, M., and Rodriguez-Pombo, P. (2002). Transfection screening for defects in the PCCA and PCCB genes encoding propionyl-CoA carboxylase subunits. *Mol. Genet. Metabol.* 75, 276–279.
58. Guenzel, A.J., Hofherr, S.E., Hillestad, M., Barry, M., Weaver, E., Venezia, S., Kraus, J.P., Matern, D., and Barry, M.A. (2013). Generation of a hypomorphic model of propionic acidemia amenable to gene therapy testing. *Mol. Ther.* 21, 1316–1323.
59. Jiang, L., Park, J.S., Yin, L., Laureano, R., Jacquinet, E., Yang, J., Liang, S., Frassetto, A., Zhuo, J., Yan, X., et al. (2020). Dual mRNA therapy restores metabolic function in long-term studies in mice with propionic acidemia. *Nat. Commun.* 11, 5339.
60. Arechavala-Gomez, V., Graham, I.R., Popplewell, L.J., Adams, A.M., Aartsma-Rus, A., Kinali, M., Morgan, J.E., van Deutekom, J.C., Wilton, S.D., Dickson, G., and Muntoni, F. (2007). Comparative analysis of antisense oligonucleotide sequences for targeted skipping of exon 51 during dystrophin pre-mRNA splicing in human muscle. *Hum. Gene Ther.* 18, 798–810.
61. Cirak, S., Arechavala-Gomez, V., Guglieri, M., Feng, L., Torelli, S., Anthony, K., Abbs, S., Garralda, M.E., Bourke, J., Wells, D.J., et al. (2011). Exon skipping and dystrophin restoration in patients with Duchenne muscular dystrophy after systemic phosphorodiamidate morpholino oligomer treatment: an open-label, phase 2, dose-escalation study. *Lancet* 378, 595–605.
62. Hua, Y., Vickers, T.A., Okunola, H.L., Bennett, C.F., and Krainer, A.R. (2008). Antisense Masking of an hnRNP A1/A2 Intronic Splicing Silencer Corrects SMN2 Splicing in Transgenic Mice. *Am. J. Hum. Genet.* 82, 834–848.
63. Finkel, R.S., Chiriboga, C.A., Vajsa, J., Day, J.W., Montes, J., De Vivo, D.C., Yamashita, M., Rigo, F., Hung, G., Schneider, E., et al. (2016). Treatment of infantile-onset spinal muscular atrophy with nusinersen: a phase 2, open-label, dose-escalation study. *Lancet* 388, 3017–3026.
64. Kim, J., Hu, C., Moufawad El Achkar, C., Black, L.E., Douville, J., Larson, A., Pendergast, M.K., Goldkind, S.F., Lee, E.A., Kuniyoshi, A., et al. (2019). Patient-Customized Oligonucleotide Therapy for a Rare Genetic Disease. *N. Engl. J. Med.* 381, 1644–1652.
65. Brasil, S., Vicelli, H.M., Meili, D., Rassi, A., Desviat, L.R., Pérez, B., Ugarte, M., and Thöny, B. (2011). Pseudoexon exclusion by antisense therapy in 6-pyruvoyl-tetrahydropterin synthase deficiency. *Hum. Mutat.* 32, 1019–1027.
66. Ferri, L., Covello, G., Caciotti, A., Guerrini, R., Denti, M.A., and Morrone, A. (2016). Double-target Antisense U1snRNAs Correct Mis-splicing Due to c.639+861C>T and c.639+919G>A GLA Deep Intronic Mutations. *Mol. Ther. Nucleic Acids* 5, e380.
67. Kumar, R., Corbett, M.A., Smith, N.J.C., Hock, D.H., Kikhtyak, Z., Semcesen, L.N., Morimoto, A., Lee, S., Stroud, D.A., Gleason, J.G., et al. (2022). Oligonucleotide correction of an intronic TIMMDC1 variant in cells of patients with severe neurodegenerative disorder. *NPJ Genom. Med.* 7, 9.
68. Gökirmak, T., Nikan, M., Wiechmann, S., Prakash, T.P., Tanowitz, M., and Seth, P.P. (2021). Overcoming the challenges of tissue delivery for oligonucleotide therapeutics. *Trends Pharmacol. Sci.* 42, 588–604.
69. Geary, R.S., Norris, D., Yu, R., and Bennett, C.F. (2015). Pharmacokinetics, bio-distribution and cell uptake of antisense oligonucleotides. *Adv. Drug Deliv. Rev.* 87, 46–51.
70. Prakash, T.P., Graham, M.J., Yu, J., Carty, R., Low, A., Chappell, A., Schmidt, K., Zhao, C., Aghajani, M., Murray, H.F., et al. (2014). Targeted delivery of antisense oligonucleotides to hepatocytes using triantennary N-acetyl galactosamine improves potency 10-fold in mice. *Nucleic Acids Res.* 42, 8796–8807.
71. Huang, Y. (2017). Preclinical and Clinical Advances of GalNAc-Decorated Nucleic Acid Therapeutics. *Mol. Ther. Nucleic Acids* 6, 116–132.
72. Miyazaki, T., Ohura, T., Kobayashi, M., Shigematsu, Y., Yamaguchi, S., Suzuki, Y., Hata, I., Aoki, Y., Yang, X., Minjares, C., et al. (2001). Fatal propionic acidemia in mice lacking propionyl-CoA carboxylase and its rescue by postnatal, liver-specific supplementation via a transgene. *J. Biol. Chem.* 276, 35995–35999.
73. Clavero, S., Pérez, B., Rincón, A., Ugarte, M., and Desviat, L.R. (2004). Qualitative and quantitative analysis of the effect of splicing mutations in propionic acidemia underlying non-severe phenotypes. *Hum. Genet.* 115, 239–247.
74. Bychkov, I., Galushkin, A., Filatova, A., Nekrasov, A., Kurkina, M., Baydakova, G., Ilyushkina, A., Skoblov, M., and Zakharova, E. (2021). Functional Analysis of the PCCA and PCCB Gene Variants Predicted to Affect Splicing. *Int. J. Mol. Sci.* 22, 4154.
75. Han, Z., Chen, C., Christiansen, A., Ji, S., Lin, Q., Anumonwo, C., Liu, C., Leiser, S.C., Meena, N., Aznar, L., et al. (2020). Antisense oligonucleotides increase Scn1a expression and reduce seizures and SUDEP incidence in a mouse model of Dravet syndrome. *Sci. Transl. Med.* 12, eaaz6100.
76. Carvill, G.L., Engel, K.L., Ramamurthy, A., Cochran, J.N., Roovers, J., Stamberger, H., Lim, N., Schneider, A.L., Hollingsworth, G., Holder, D.H., et al. (2018). Aberrant Inclusion of a Poison Exon Causes Dravet Syndrome and Related SCN1A-Associated Genetic Epilepsies. *Am. J. Hum. Genet.* 103, 1022–1029.
77. Richard, E., Desviat, L.R., Pérez, B., Pérez-Cerdá, C., and Ugarte, M. (1999). Genetic heterogeneity in propionic acidemia patients with alpha-subunit defects. Identification of five novel mutations, one of them causing instability of the protein. *Biochim. Biophys. Acta* 1453, 351–358.
78. Oliveros, J.C., Franch, M., Tabas-Madrid, D., San-León, D., Montoliu, L., Cubas, P., and Pazos, F. (2016). Breaking-Cas-interactive design of guide RNAs for CRISPR-Cas experiments for ENSEMBL genomes. *Nucleic Acids Res.* 44, W267–W271.
79. Suormala, T., Wick, H., Bonjour, J.P., and Baumgartner, E.R. (1985). Rapid differential diagnosis of carboxylase deficiencies and evaluation for biotin-responsiveness in a single blood sample. *Clin. Chim. Acta* 145, 151–162.
80. Frederiksen, S.B., Holm, L.L., Larsen, M.R., Doktor, T.K., Andersen, H.S., Hastings, M.L., Hua, Y., Krainer, A.R., and Andresen, B.S. (2021). Identification of SRSF10 as a regulator of SMN2 ISS-N1. *Hum. Mutat.* 42, 246–260.
81. Dobin, A., Davis, C.A., Schlesinger, F., Drenkow, J., Zaleski, C., Jha, S., Batut, P., Chaisson, M., and Gingeras, T.R. (2013). STAR: ultrafast universal RNA-seq aligner. *Bioinformatics* 29, 15–21.
82. Love, M.I., Huber, W., and Anders, S. (2014). Moderated estimation of fold change and dispersion for RNA-seq data with DESeq2. *Genome Biol.* 15, 550.
83. Cunningham, F., Achuthan, P., Akanni, W., Allen, J., Amode, M.R., Armean, I.M., Bennett, R., Bhari, J., Billis, K., Boddie, S., et al. (2019). Ensembl 2019. *Nucleic Acids Res.* 47, D745–D751.
84. Pluskal, T., Castillo, S., Villar-Briones, A., and Orešič, M. (2010). MZmine 2: modular framework for processing, visualizing, and analyzing mass spectrometry-based molecular profile data. *BMC Bioinf.* 11, 395.
85. Salek, R.M., Haug, K., and Steinbeck, C. (2013). Dissemination of metabolomics results: role of MetaboLights and COSMOS. *GigaScience* 2, 8.
86. Luan, H., Ji, F., Chen, Y., and Cai, Z. (2018). A streamlined tool for signal drift correction and interpretations of quantitative mass spectrometry-based omics data. *Anal. Chim. Acta* 1036, 66–72.
87. Chong, J., Wishart, D.S., and Xia, J. (2019). Using MetaboAnalyst 4.0 for Comprehensive and Integrative Metabolomics Data Analysis. *Curr. Protoc. Bioinforma.* 68, e86.
88. Cartegni, L., Wang, J., Zhu, Z., Zhang, M.Q., and Krainer, A.R. (2003). ESEfinder: a web resource to identify exonic splicing enhancers. *Nucleic Acids Res.* 31, 3568–3571.
89. Smith, P.J., Zhang, C., Wang, J., Chew, S.L., Zhang, M.Q., and Krainer, A.R. (2006). An increased specificity score matrix for the prediction of SF2/ASF-specific exonic splicing enhancers. *Hum. Mol. Genet.* 15, 2490–2508.
90. Yeo, G., and Burge, C.B. (2004). Maximum Entropy Modeling of Short Sequence Motifs with Applications to RNA Splicing Signals. *J. Comput. Biol.* 11, 377–394.